Comparative Anatomical Limits of CART-Cell Delivery to Tumours in Mice and Men

Liam V Brown[a,b*], Eamonn A Gaffney[a], Ann Ager[c], Jonathan Wagg[d], and Mark C Coles[b*]

[a]Wolfson Centre For Mathematical Biology, Mathematical Institute, University of Oxford
[b]Kennedy Institute of Rheumatology, University of Oxford
[c]Systems Immunity University Research Institute and Division of Infection and Immunity, School of Medicine, Cardiff University
[d]Pharmaceutical Sciences–Clinical Pharmacology, Roche Innovation Center Basel
[*]*Corresponding authors: LVB: (last-name)@maths.ox.ac.uk. MCC: mark.coles@kennedy.ox.ac.uk, (+44)1865 612675*

September 5, 2019

Abstract

CART (Chimeric Antigen Receptor T)-cells are approved for treatment of several leukaemia and lymphoma indications. However, this therapeutic modality has not delivered comparable clinical efficacy for solid tumour indications despite promising preclinical outcomes in mouse solid tumour models. Lower rates of effective CART-cell delivery to solid tumours in humans as compared to human haematological malignancies and/or solid tumours in mice might partially explain these divergent outcomes. As the initial delivery of CART-cells to tumour tissue is mediated by the circulatory system, we developed *in silico* models of the human, rat and mouse circulatory systems. Model structure and parameterisation were informed by an extensive body of published comparative anatomical and physiological studies and associated experimental data. Models were used to estimate the species-dependent upper limit and variation of delivery rates of blood borne immune cells, such as T- and NK cells, to tumour tissue across different organs and species. Large cross-species differences in absolute delivery rates to organs were identified. Estimated maximum delivery rates were up to 10,000-fold greater in mice than humans, yet reported administered CART-cell doses were typically only 10-100 times lower in mice. This suggests that higher human CART-doses may be needed to drive efficacy comparable to that observed in preclinical solid tumour mice models. Accordingly, we posit that a more quantitative analysis of species- and organ-specific immune cell delivery rates and how they may be pharmacologically optimised will be key to unlocking the potential of engineered T-cells for solid tumours.

1 Introduction

Cellular therapies such as CART-cells have shown clinical efficacy against haematological malignancies and are approved for several leukaemias and lymphomas [1, 2]. Despite efficacy seen in pre-clinical models, this success has not yet been matched for solid tumours and a suitable dosing strategy to maximise efficacy remains uncertain [3–8]. Typical response curves (amount of CART-cell transgene observed in blood versus time) in patients with haematological disorders are marked by an initial cellular expansion (typically 100-1000-fold [9]), due to the large numbers of CART and target cells colocalising in readily accessible tissues. Expansion increases the effective cellular dose entering and proliferating within compartments with lower perfusion or less efficient access, which can drive the clearance of target cells required to achieve complete responses in these compartments. In solid tumours, relatively few target cells are in readily accessible compartments, whether due to poor perfusion or barriers to extravasation, preventing a strong initial expansion of CART-cells. Tumour regression is achieved when the rate of tumour clearance is greater than that of tumour growth, including in the least perfused/accessible tumour lesions. In this context, tumour clearance is a numbers game and the relative lack of success for solid tumours may be due to lower effective CART-cell doses, since the number of accessible target cells is too low to drive the early cellular expansion that, in the case of haematological malignancies, increases the effective dose.

The delivery rate of cells to different compartments of the body will likely be of importance in CART-cell or eTCR (engineered T-cell receptor) responses. For intravenous (iv) administration, cells are delivered by the circulatory system. Systematic quantitation of the variation of vascular delivery rates across organs, tumour types and species will improve understanding of comparative preclinical and clinical outcomes and inform improved dosing strategies. Physiologically-based pharmacokinetic modelling (PBPK)

has been used extensively to predict drug concentration profiles and their variability across different tissues and individuals, to estimate the efficacy of clinical dosing regimens (for recent reviews, see [10–12]). PBPK models have been used in drug development since 2000 and are readily accepted as providing supporting information by both the US Food and Drug Administration and the European Medicines Agency. They have also been used to study T-cell trafficking, for example to determine the strength of the abscopal affect and influence of metastases on the primary tumour [13, 14] and to study localisation of T-cell therapies [15–18], but we have not seen an attempt to quantify and compare delivery rates of bioengineered T-cells across organs and species, the aim of the present work.

We have produced mathematical models to describe human, mouse and rat circulatory systems, including relevant organ and tumour tissue parameterised by anatomical data [19–24]. They have been used to calculate the upper bounds of cellular delivery from the circulation into each organ, considering only tissue perfusion and not factors such as tissue-specific extravasation probabilities. Maximum delivery rates exhibited extreme differences by species. The delivery rate of cells per minute per mm^3 to lungs is 10,000-fold higher in mice than humans, yet typical doses of CART cells given to experimental mice are only 100-fold less than those in the clinic. This may partially explain the lack of success seen against solid tumours reported to date.

2 Methods

ODE model: A simplified schematic of the mathematical model (Figure 1a) outlines how T-cells flow from the heart to the vasculature of different organs and return, with a proportion e_o of T-cells passing through each organ o extravasating into that organ's interstitial space. Extravasated cells transit via lymphatics to lymph nodes and return to circulation, except for the spleen, from which cells return directly to circulation. For the purposes of computation, one organ is defined as the tumour bearing organ, containing a $1mm^3$ tumour ('tmr') tissue volume. We consider this volume either as healthy or tumour tissue, to find how delivery rates to each differ across organs and species. The *maximum* delivery rate of cells to a target volume in each organ o is the case for which $e_o = 1.0$ in that region. This rate is insensitive to the values $e_{o'}$ in any other organ o' if the blood concentration of T-cells is constant (see sensitivity analysis in supplementary section 2.4). Thus, the maximum delivery rate of T-cells per mm^3 is calculated for each organ in turn by setting e to zero everywhere but for a volume of $1mm^3$ in the organ of interest (Figure 1b). This results in a nearly constant T-cell blood concentration and thus correct calculation of the maximum rate of cell delivery to a tumour in each organ. A more detailed description of equations and parameter values used in the model is given in supplementary section 1.1. The remainder of this text will refer simply to "delivery rates", but this is more precisely "maximum delivery rates per mm^3 of tissue (or tumour)".
Predicted T-cell delivery rates are dependent on assumed anatomical parameters (blood flow, blood volume and organ volume). We collected several anatomical reference banks from the literature [19–24], each with slightly differing fractional blood flows and volumes. To remove selection bias, the model was run multiple times ($n = 100$ per organ per species), selecting uniformly random values for each anatomical parameter from the range of literature values, and means and standard deviations were calculated from the estimated delivery rates.
Sensitivity analysis: Random values of extravasation probabilities of T-cells into all 20 organs and the tumour were chosen. The extravasation rate of T-cells into tumours in each organ was calculated by selecting each organ to be tumour-bearing in turn. This process was repeated over 1000 simulations and data used to grow a random forest, as detailed in supplementary section 2.4.
Data sharing statement: For additional parameter sets and code, please contact LVB. These will be made available in a public repository.

3 Results

3.1 CART-cell delivery to organs in humans, mice and rats

The model was used to compare the delivery rate (cells/min/mm^3) of a typical number of CART-cells used in the clinic (10^8 [25, 26]) to healthy tissues in different human, rat and mouse organs. The results (Table 1) are approximately equal to the product of the organ perfusion and CART-cell blood concentration, with some deviation due to the details of the circulation or limited organ size. Flow from both the hepatic artery and portal vein are included in delivery rates to the liver, and the pulmonary circuit and lung blood supply are both included for lung rates. The difference in delivery rates to the same organ in different species can be extreme, with predicted absolute lung delivery rates per volume in the mouse 17,000 times higher than in humans if the same number of CART-cells is administered to each species (obtained by dividing 3,000,000/180 from Table 1). Should a constant blood concentration of endogenous cells be considered instead of a constant number, then rates per volume depend on both organ perfusion and total blood volume, and the absolute delivery rates for mice are 8 times higher than in humans. These data suggest a novel approach for scaling murine dosages to humans, by ensuring that the same cellular delivery rate to tissues of interest is achieved. Results of Table 1 were used to calculate the CART-cell doses (introduced cell numbers) required to obtain the same delivery rates

in humans as in mice given a typical pre-clinical dose of 10^7 CART-cells. Equivalent doses are organ-specific, and most are of order 10^{10} to 10^{11} cells (Table 2).

To illustrate organ-specific scaling and allow interspecies comparison of the distribution of delivery rates across organs, predicted delivery rates in Table 1 were subsequently normalised such that the sum of the mean predictions within each species is 1.0. The mean and standard deviation of normalised delivery rates are plotted in Figure 2. The distributions share similarities but otherwise the relative rates scale differently for each organ. For each species, the lung has the highest delivery rate, followed by the kidneys.

3.2 CART-cell delivery to human tumours

Predicted maximum delivery rates per mm^3 described above assume that organ perfusion is homogeneous. However, a tumour may have different perfusion to healthy tissues. The literature was surveyed to quantify the variability of human tumour perfusion (supplementary figure 2) and to implement tumour-type-specific perfusion into the model. The model was run many times ($n = 150$ per organ) with uniformly random values for all organ parameters and normally distributed values of tumour perfusion from the extracted literature data, to determine a mean and standard deviation of predicted delivery rates for CART-cells to human tumours. These rates are shown in Figure 3, along with the corresponding delivery rates under the assumption of homogeneous perfusion (*i.e.* to healthy tissue; blue dotted boxes). The rank order of delivery rates to tumour and healthy tissues are very different. In most cases, the average of predicted delivery rates for tumour tissue is similar to or less than that for healthy tissue, but in some cases (*e.g.* the skin) it is considerably greater. However, their variation is considerable; extreme values (whiskers in the plot) vary over many orders of magnitude above and below that of the corresponding healthy tissue, for most organs.

3.3 Comparison to PET imaging and radiography data

The validity of predicted maximum delivery rates can be checked by comparing data from PET imaging and radiography studies in humans and rodents, in which cell localisation at early time points has been recorded. The use of an early time point is critical, as it shows the location of cells that are still in the blood or recently extravasated into an organ, before they drain back into the blood and recirculate. At later time points, localisation is a function of both cell delivery to organs and return to circulation. The delivery of radiolabelled natural killer cells from the bloodstream into individual organs has been studied in rats [27] and in human patients [28, 29]. These data are presented in Figure 4 and compared to predictions from Table 1. Patients in the human study were given 10^8 to 10^9 cells; the average fraction found in the liver at the first time point (30 minutes) was 8.9%. This corresponds to approximately 4.5×10^7 cells. The rats were given 10^6 to 10^7 cells; the average fraction found in the liver at the first time point (30 minutes) was 23.0%, or 1.2×10^6 cells. Adjusting the rat numbers to the same dose gives 1.2×10^8 cells. If we then assume a liver volume of 1700ml in humans and 10ml in rats, we obtain cell number per volume in the liver: 2.6×10^4 in humans and 1.1×10^7 in rats, a ratio of 429. The ratio of maximum delivery rates predicted by our model is 546 (Table 1), 1.27-fold larger than expected from the data. Repeating this analysis for the lungs and spleen gives experimental ratios 2.0-fold less than predicted by the model (see Figure 4).

4 Discussion

This study aimed to quantify physiological constraints on the rate of CART-cell delivery by the blood to target tissues in different species, to better predict appropriate clinical CART-cell doses from pre-clinical data. It has focused on tumour infiltration, though the methodology may also apply to other therapeutic areas, including immune-related adverse event prediction. Values were calculated assuming that 10^8 T-cells are introduced; however, delivery rates due to any other desired number or blood concentration of cells could be calculated by multiplying results by the ratio of the desired number to 10^8 or multiplying blood concentration by the total blood volume in the target species. Although models to predict expansion of a T-cell population have been studied in the past [9, 30], it is difficult to quantify cellular proliferation in or fractional recirculation from a given tissue. However, a maximum rate of delivery due to anatomy can be estimated with greater confidence, thus proliferation was not considered.

4.1 Organ-specific delivery rates and their variation

Results predict that the highest CART-cell delivery rates are in organs with the highest perfusion: the lungs and kidneys in humans (Figure 2). When tumour-specific perfusion is considered (Figure 3), it is the kidneys, skin, large intestine and lungs that are predicted to have the highest delivery rates per mm^3, consistent with non-cellular immunotherapies (IL-2 and checkpoint blockade) having the highest efficacy in kidney, skin, colon and lung tumours [31–36], and the hypothesis that efficacy is driven in part by tissue perfusion. For cellular therapies including CART-cells, vascular delivery should similarly correlate with efficacy, with the additional factor that T-cells must extravasate into target tissues. Both naïve and *ex vivo* T-cells preferentially extravasate into lymph nodes, spleen and liver [37–39], consistent with CART-cell efficacy in haematological disorders but not solid tumours [1, 25, 26]. Predicted mean

delivery rates into tumours exceed those to healthy tissue for only a minority of organs (Figure 3), including the skin. Predicted delivery rates to tumours in the skin vary over many orders of magnitude but are usually greater than those for healthy tissue. Healthy skin is not usually highly perfused and contains shunts to control blood flow in response to temperature. Most anatomical data for the skin describes the organ at rest and at room temperature with no inflammation, meaning most shunts will be open. Tumour tissue can increase its perfusion through inflammation or angiogenesis and likely subverts these shunts, which could explain the greater mean and variation in predicted delivery rates for skin tumours. Liver and kidney tissues are highly perfused at rest, which are unlikely to be improved by random tumour angiogenesis; accordingly, predicted delivery rates to tumours in these organs do not exceed healthy tissue. Predictions for red bone marrow indicate that tumour perfusion can greatly outstrip healthy tissue perfusion. Though surprising, this result is consistent with studies in which bone perfusion was measured in healthy control bone and tumour sites in patients with bone cancers and metastases [40]. Finally, predicted delivery rates to lung tumours may or may not exceed that of healthy tissue, depending on whether the pulmonary circuit is assumed to contribute to tumour blood supply (blue dotted box) or not (green dashed box).

Both figures show that predicted delivery rates are highly variable, which may be caused by differences in experimental techniques or individual variation. Physiological differences and behaviour both impact blood flow distributions; blood flow to the mesentery increases after a meal, muscles during exercise, or the skin in response to temperature. This effect is utilised in the clinic to prevent hair loss in chemotherapy patients by cooling the scalp. CART-cell therapies could be targeted to organs such as the mesentery or skin through meal consumption or temperature control, and tumour-specific blood flow could be increased with anti-angiogenic therapies (*e.g.* Avastin). Both human and rodent anatomical parameters vary, impacting any results that depend on anatomical parameters. If variability is not captured and/or care is not taken to control factors that alter blood flows (*e.g.* anaesthesia, exercise or the time of day [41]), then comparison of data sets may be invalid. Ideally, any study making use of blood flows and organ volumes should consider multiple measurements and include 'error' bars to indicate variation.

4.2 Species-specific delivery rates and dosage scaling

Relative delivery rates are distributed differently across organs in each species, meaning that dose scaling is organ-specific (Figure 2, Table 1). Predicted absolute delivery rates of the same dose of CART-cells (10^8) exhibit extreme differences in different species, with delivery per volume to mouse lungs 17,000 times higher than in humans, largely because of the difference in total blood volumes between mice (1.5mL) and humans (5L). To test model predictions, we analysed published PET imaging and radiography studies of natural killer (NK) cells in humans and rats [27–29] and calculated the cell numbers present in various organs at early time points (Section 3.3). The human/rat ratios of NK cells per volume in the lungs, liver and spleen 30 minutes after infusion were compared to the human/rat ratios of predicted maximum delivery rates from our model. The measured localisation ratios are 1.3 to 2.0-fold greater than predictions. Such small discrepancies are not unexpected, as delivery *rate* ratios would only equal localisation ratios if the blood concentration of NK cells and hence delivery rates were constant. However, the earliest experimental time point is 30 minutes, providing sufficient time for blood recirculation (as cardiac output/minute is greater than total blood volume in humans and rats). The rates of extravasation and return in each organ may differ between humans and rats, and the experimental technique and total amount of radioactivity at the first time point differs between the two studies. Aside from these considerations, these specific model predictions are consistent with the available observations.

Despite the considerably greater delivery rates of cells in mice than humans, typical doses (cell numbers) introduced to mice are not considerably lower than those given to humans. Most patients are given CART-cell dosages between 10^7 and 10^9 cells [25, 26], whilst mouse studies have used (*e.g.*) two doses of 1 to 2.5×10^6 cells a week apart [6], two doses of 10^7 cells a week apart [3], and a single dose of 10^7 cells [4]. To illustrate how large these doses are, we calculated equivalent human dosages that would yield the same absolute delivery rates in humans as in a mouse given 10^7 CART-cells (Table 2). The resulting doses range between 10^{10} and 10^{11} T-cells, much higher than typical clinical doses and many dose escalation studies [26]. This may explain why pre-clinical success does not always translate to the clinic. A pre-clinical study of a CEA CART-cell therapy resulted in regression of subcutaneous tumours in mice with a dose of 5×10^6 cells (equivalent to 1.7×10^{10} in humans) [42]. In another study, a CART-cell therapy restricted the growth of pancreatic tumours in all treated mice to below the limit of detection with a dose of 10^7 cells (equivalent to 4.5×10^{10} in humans) [43]. In the clinic, a study of CEA CART-cells against colorectal cancer [44] escalated doses between 10^7 and 10^{10}. The authors found that the lower doses did not stop tumour progression (in 3 of 14 of presented patients) and higher doses achieved only stable disease. Our results suggest that dosages of order 10^{10} cells would be required to drive tumour regression at the primary site, and 10^{11} would be required for the lung metastases. Clinical studies in which Tumour Infiltrating Lymphocytes (TILs) were introduced in greater numbers (10^9 to 10^{11}) [45–48] and in which CART-cells were introduced regionally (bypassing trafficking via the bloodstream) [25] are associated with greater efficacy.

In patients with advanced metastatic disease, CART-cell dosage must be sufficient to drive tumour regression at the least perfused and/or the fastest growing site. To avoid dosage-linked increases in adverse events such as cytokine release or encephalopathy syndromes, methods to increase the effective dose on-site and not elsewhere should be considered, including alternate modes of

administration, triggering proliferation at sites of interest, coadministration of inhibitors (e.g. anti-IL6), or interventions to alter blood flows described in Section 4.1.

The numbers presented here compare organs like-for-like between mice and humans, but scaling is more uncertain for xenografts. The ratio of the maximum delivery rate per volume to skin tissue between mice and humans is 2 if the same blood concentration of immune cells is assumed, or 3400 if the same number of immune cells is assumed (calculated from Table 1). The ratio of delivery rates per volume to mouse skin versus human kidney tissue, meanwhile, is 0.05 if the same concentration of cells is used, or 100 if the same number of immune cells is assumed. A previous study [49] has shown that small xenografts have similar local perfusion to the original tissue, but larger xenografts have reduced perfusion relative to normal tissue. This non-linearity further confounds extrapolation of preclinical results. This may explain part of the historically observed difficulties in the clinical translation of preclinical mouse xenograft model results [50]. In addition to consideration of physiological and immunological differences (such as the adhesion molecules required for T-cell extravasation), interpretation of pre-clinical therapeutic success requires dosages to be appropriately scaled to humans. A model that considers organ-specific blood flow and volumes across species can be used to more precisely estimate likely efficacious human doses.

4.3 Model refinement and further considerations

Model predictions are the maximum rate of CART-cell delivery per volume (cells/min/mm^3) to organs and tumours, based on only organ blood flows and volumes. Refining these predictions requires quantification of CART-cell proliferation and organ-specific homing. The probability of T-cell extravasation differs by location and cell type. Naïve T-cells extravasate mainly into the lymph nodes or spleen and activated cells have a higher probability of extravasating into non-lymphoid tissues [37, 51], distributed according to upregulated homing receptors (*e.g.* L-selectin or CCR7 [52]). These probabilities may differ across species (*e.g.* homing receptor CXCR1 is present in humans but not mice [53]), further limiting inter-species extrapolation of pre-clinical results. Homing receptor density, vessel normalisation and hence homing probabilities may further differ in tumour tissue, particularly following therapies such as Avastin [54, 55].

Another challenge for CART-cells in solid tumours is the identification of suitable target antigen. The ideal antigen is highly expressed on tumour cells and not expressed on healthy cells elsewhere. A typical target for B-cell malignancies is CD19 [26], as it is expressed by the entire pool of B-cells and is limited almost exclusively to B-cells. Several different antigens have been targeted for solid tumours, but with limited success (for example, GD2 has had encouraging results [26]). Target antigen may only be expressed by a subset of tumour cells and may not be sufficiently rare elsewhere in the body. For example, CAIX is expressed in some renal cell carcinomas, but it is also expressed in the liver bile duct resulting in on-target, off-tumour toxicities in a phase III trial [56]. Tumours may evolve to reduce expression of target antigen in response to successful T-cell killing, reducing the rate of tumour elimination or promoting outgrowth of therapy-resistant cells. Although these considerations are a barrier to treatment success, the rate at which cells can be delivered is a parallel and important factor. CART-cells that are specific for an antigen that is expressed on most tumour cells will not drive tumour regression if their kill rate is lower than the tumour growth rate, given the combined rates of T-cell delivery and proliferation. On the other hand, CART-cells specific for a rarer antigen may drive tumour regression if they arrive in sufficient numbers to eliminate all cells carrying that antigen, subsequently proliferating to greater numbers to drive regression at more restricted sites and/or drive a secondary response against one or more other antigens (*i.e.* epitope spread). Like T-cell delivery rates and T-cell extravasation probabilities, typical tumour growth rates are species, organ and individual specific. Together, these considerations show that tumour immunotherapy is a numbers game and hence quantitative studies can be a useful tool for understanding the translational gap between pre-clinical and clinical outcomes.

5 Conclusions

Dynamic models of human, rat and mouse circulatory systems were implemented to predict CART-cell delivery to human tumours, and to human, rat and mouse organs. Models show up to 10,000-fold increased CART-cell delivery per volume in mice than humans, while typical clinical cell therapy dosages are 100-fold less than typical pre-clinical doses. These numbers were consistent with experimental studies of NK cell localisation. These predictions could partially explain why pre-clinical models of solid tumour clearance by CART-cells show greater efficacy than in humans. Dosage scaling was found to be organ-specific and is particularly hard to quantify for xenografts, confounding the interpretation of pre-clinical results and lowering their potential clinical value, which is an important consideration in the context of the reduction and replacement of animal experiments. Control of tumour and organ-specific blood flow through exercise, circadian timing, food consumption or vascular normalisation agents could increase cellular delivery to tumour sites without raising risk of adverse outcomes. Cellular kinetic and dynamic models will lead to better understanding of how pre-clinical outcomes translate to the clinic, and hence better determination of appropriate clinical dosages and treatment strategies for cell-based therapies.

Acknowledgements

This research was supported by funding from a Clarendon Scholarship, Hoffman-La Roche and the Engineering and Physical Sciences Research Council (EPSRC), grant number EP/L016044/1.

Author contributions

LVB designed the model code, did the analysis and wrote the manuscript. All other authors supervised, advised and edited the manuscript.

Conflict of interest disclosure

JW is an employee and shareholder of Hoffman-La Roche. LVB has previously completed an internship at that same company.

References

[1] David Pettitt, Zeeshaan Arshad, James Smith, Tijana Stanic, Georg Holländer, and David Brindley. CAR-T Cells: A Systematic Review and Mixed Methods Analysis of the Clinical Trial Landscape. *Molecular Therapy*, 26(2):342–353, 2018. doi: 10.1016/j.ymthe.2017.10.019.

[2] Charlotte Graham, Rebecca Hewitson, Antonio Pagliuca, and Reuben Benjamin. Cancer immunotherapy with CAR-T cells - Behold the future. *Clinical Medicine, Journal of the Royal College of Physicians of London*, 18(4):324–328, 2018. ISSN 14734893. doi: 10.7861/clinmedicine.18-4-324.

[3] He Li, Yao Huang, Du-Qing Jiang, Lian-Zhen Cui, Zhou He, Chao Wang, Zhi-Wei Zhang, Hai-Li Zhu, Yong-Mei Ding, Lin-Fang Li, Qiang Li, Hua-Jun Jin, and Qi-Jun Qian. Antitumor activity of EGFR-specific CAR T cells against non-small-cell lung cancer cells in vitro and in mice. *Cell Death & Disease*, 9(2): 177, 2018. ISSN 2041-4889. doi: 10.1038/s41419-017-0238-6.

[4] Nobuhiro Nishio, Iulia Diaconu, Hao Liu, Vincenzo Cerullo, Ignazio Caruana, Valentina Hoyos, Lisa Bouchier-Hayes, Barbara Savoldo, and Gianpietro Dotti. Armed oncolytic virus enhances immune functions of chimeric antigen receptor-modified T cells in solid tumors. *Cancer Research*, 74(18):5195–5205, 2014. ISSN 15387445. doi: 10.1158/0008-5472.CAN-14-0697.

[5] Kheng Newick, Edmund Moon, and Steven M. Albelda. Chimeric antigen receptor T-cell therapy for solid tumors. *Molecular Therapy - Oncolytics*, 3(October 2015):16006, 2016. ISSN 23727705. doi: 10.1038/mto.2016.6.

[6] Mauro P. Avanzi, Oladapo Yeku, Xinghuo Li, Dinali P. Wijewarnasuriya, Dayenne G. van Leeuwen, Kenneth Cheung, Hyebin Park, Terence J. Purdon, Anthony F. Daniyan, Matthew H. Spitzer, and Renier J. Brentjens. Engineered Tumor-Targeted T Cells Mediate Enhanced Anti-Tumor Efficacy Both Directly and through Activation of the Endogenous Immune System. *Cell Reports*, 23(7):2130–2141, 2018. ISSN 22111247. doi: 10.1016/j.celrep.2018.04.051.

[7] Jeffrey R. Sachs, Kapil Mayawala, Satvik Gadamsetty, Soonmo Peter Kang, and Dinesh P. de Alwis. Optimal Dosing for Targeted Therapies in Oncology: Drug Development Cases Leading by Example. *Clin. Cancer Res.*, 22(6):1318–1324, Mar 2016. ISSN 1078-0432. doi: 10.1158/1078-0432.CCR-15-1295.

[8] Yan Ji, Jin Y. Jin, David M. Hyman, Geoffrey Kim, and Ajit Suri. Challenges and Opportunities in Dose Finding in Oncology and Immuno-oncology. *Clin. Transl. Sci.*, 11(4):345, Jul 2018. doi: 10.1111/cts.12540.

[9] Andrew M. Stein, Stephan A. Grupp, John E. Levine, Theodore W. Laetsch, Michael A. Pulsipher, Michael W. Boyer, Keith J. August, Bruce L. Levine, Lori Tomassian, Sweta Shah, Mimi Leung, Pai-Hsi Huang, Rakesh Awasthi, Karen Thudium Mueller, Patricia A. Wood, and Carl H. June. Tisagenlecleucel Model-Based Cellular Kinetic Analysis of Chimeric Antigen Receptor–T Cells. *CPT Pharmacometrics Syst. Pharmacol.*, 8(5):285–295, May 2019. ISSN 2163-8306. doi: 10.1002/psp4.12388.

[10] K Yoshida, N Budha, and J. Jin. Impact of Physiologically Based Pharmacokinetic Models on Regulatory Reviews and Product Labels: Frequent Utilization in the Field of Oncology. *Clinical Pharmacology and Therapeutics*, 101(5):597–602, 2017. doi: 10.1002/cpt.622.

[11] Teerachat Saeheng, Kesara Na-Bangchang, and Juntra Karbwang. Utility of physiologically based pharmacokinetic (PBPK) modeling in oncology drug development and its accuracy: a systematic review. *European Journal of Clinical Pharmacology*, July 2018. ISSN 0031-6970. doi: 10.1007/s00228-018-2513-6.

[12] Mohamad Shebley, Punam Sandhu, Arian Emami Riedmaier, Masoud Jamei, Rangaraj Narayanan, Aarti Patel, Sheila Annie Peters, Venkatesh Pilla Reddy, Ming Zheng, Loeckie Zwart, Maud Beneton, Francois Bouzom, Jun Chen, Yuan Chen, Yumi Cleary, Christiane Collins, Gemma L. Dickinson, Nassim Djebli, Heidi J. Einolf, Iain Gardner, Felix Huth, Faraz Kazmi, Feras Khalil, Jing Lin, Aleksandrs Odinecs, Chirag Patel, Haojing Rong, Edgar Schuck, Pradeep Sharma, Shu-Pei Wu, Yang Xu, Shinji Yamazaki, Kenta Yoshida, and Malcolm Rowland. Physiologically based pharmacokinetic model qualification and reporting procedures for regulatory submissions: A consortium perspective. *Clinical Pharmacology & Therapeutics*, 104(1):88–110, 2018. doi: 10.1002/cpt.1013.

[13] Jan T. Poleszczuk, Kimberly A. Luddy, Sotiris Prokopiou, Mark Robertson-Tessi, Eduardo G. Moros, Mayer Fishman, Julie Y. Djeu, Steven E. Finkelstein, and Heiko Enderling. Abscopal benefits of localized radiotherapy depend on activated T-cell trafficking and distribution between metastatic lesions. *Cancer Research*, 76(5):1009–1018, 2016. ISSN 15387445. doi: 10.1158/0008-5472.CAN-15-1423.

[14] Rachel Walker, Jan Poleszczuk, Shari Pilon-Thomas, Sungjune Kim, Alexander A.R.A. Anderson, Brian J. Czerniecki, Louis B. Harrison, Eduardo G. Moros, and Heiko Enderling. Immune interconnectivity of anatomically distant tumors as a potential mediator of systemic responses to local therapy. *Scientific Reports*, 8(1):1–11, 2018. ISSN 20452322. doi: 10.1038/s41598-018-27718-1.

[15] Hui Zhu, Robert J Melder, Laurence T Baxter, and Rakesh K Jain. Physiologically Based Kinetic Model of Effector Cell Biodistribution in Mammals: Implications for Adoptive Immunotherapy. (617):3771–3781, 1996.

[16] Robert J Melder, Lance L Munn, Brian R Stoll, Edgardo M Marecos, Laurence T Baxter, Ralph Weissleder, and Rakesh K Jain. Systemic distribution and tumor localization of adoptively transferred lymphocytes in mice: comparison with physiologically based pharmacokinetic model. *Neoplasia*, 4(1):3–8, 2002. ISSN 1522-8002. doi: 10.1038/sj/neo/7900209.

[17] Stuart W. Friedrich, Stephany C. Lin, Brian R. Stoll, Laurence T. Baxter, Lance L. Munn, and Rakesh K. Jain. Antibody-directed effector cell therapy of tumors: Analysis and optimization using a physiologically based pharmacokinetic model. *Neoplasia*, 4(5):449–463, 2002. ISSN 15228002. doi: 10.1038/sj.neo.7900260.

[18] Antari Khot, Satoko Matsueda, Veena A. Thomas, Richard C. Koya, and Dhaval K. Shah. Measurement and Quantitative Characterization of Whole-Body Pharmacokinetics of Exogenously Administered T Cells in Mice. *J. Pharmacol. Exp. Ther.*, 368(3):503–513, Mar 2019. ISSN 0022-3565. doi: 10.1124/jpet.118.252858.

[19] R P Brown, M D Delp, S L Lindstedt, L R Rhomberg, and R P Beliles. Physiological parameter values for physiologically based pharmacokinetic models. *Toxicology and Industrial Health*, 13(4):407–84, 1997. ISSN 0748-2337. doi: 10.1177/074823379701300401.

[20] John F. Graf, Bernhard J. Scholz, and Maria I. Zavodszky. BioDMET: A physiologically based pharmacokinetic simulation tool for assessing proposed solutions to complex biological problems. *Journal of Pharmacokinetics and Pharmacodynamics*, 39(1):37–54, 2012. ISSN 1567567X. doi: 10.1007/s10928-011-9229-x.

[21] L T Baxter, H Zhu, D G Mackensen, and R K Jain. Physiologically based pharmacokinetic model for specific and nonspecific monoclonal antibodies and fragments in normal tissues and human tumor xenografts in nude mice. *Cancer Res*, 54(6):1517–1528, 1994. ISSN 0008-5472.

[22] Dhaval K. Shah and Alison M. Betts. Towards a platform PBPK model to characterize the plasma and tissue disposition of monoclonal antibodies in preclinical species and human. *Journal of Pharmacokinetics and Pharmacodynamics*, 39(1):67–86, 2012. ISSN 1567567X. doi: 10.1007/s10928-011-9232-2.

[23] Sheila Annie Peters. *Physiologically-Based Pharmacokinetic (PBPK) Modeling and Simulations: Principles, Methods, and Applications in the Pharmaceutical Industry*. Wiley, 2012. ISBN 978-0-470-48406-7.

[24] ICRP. Basic Anatomical and Physiological Data for Use in Radiological Protection Reference Values. *ICRP Publication 89, Ann. ICRP*, 32(3-4), 2002.

[25] Praveen Sridhar and Fabio Petrocca. Regional delivery of chimeric antigen receptor (CAR) T-cells for cancer therapy. *Cancers*, 9(7):1–10, 2017. ISSN 20726694. doi: 10.3390/cancers9070092.

[26] Jessica Hartmann, Martina Schüßler-Lenz, Attilio Bondanza, and Christian J Buchholz. Clinical development of CAR T cells—challenges and opportunities in translating innovative treatment concepts. *EMBO Molecular Medicine*, 9(9):e201607485, 2017. ISSN 1757-4676. doi: 10.15252/emmm.201607485.

[27] B. Rolstad, R. B. Herberman, and C. W. Reynolds. Natural killer cell activity in the rat. V. The circulation patterns and tissue localization of peripheral blood large granular lymphocytes (LGL). *J. Immunol.*, 136(8):2800–2808, Apr 1986. ISSN 0022-1767. URL `https://www.ncbi.nlm.nih.gov/pubmed/3485674`.

[28] J.-M. Brand, B. Meller, K. Von Hof, J. Luhm, M. Bähre, H. Kirchner, and C. Frohn. Kinetics and organ distribution of allogeneic natural killer lymphocytes transfused into patients suffering from renal cell carcinoma. *Stem Cells Dev.*, 13(3):307–314, Jun 2004. ISSN 1547-3287. doi: 10.1089/154732804323099235.

[29] Birgit Meller, Christoph Frohn, Jörg-Matthias Brand, Isabel Lauer, Lutz F. Schelper, Katharina von Hof, Holger Kirchner, Eckart Richter, and Manfred Baehre. Monitoring of a new approach of immunotherapy with allogenic (111)In-labelled NK cells in patients with renal cell carcinoma. *Eur. J. Nucl. Med. Mol. Imaging*, 31(3):403–407, Mar 2004. ISSN 1619-7070. doi: 10.1007/s00259-003-1398-4.

[30] Julien Vibert and Véronique Thomas-Vaslin. Modelling T cell proliferation: Dynamics heterogeneity depending on cell differentiation, age, and genetic background. *PLoS Computational Biology*, 13(3):1–25, 2017. ISSN 15537358. doi: 10.1371/journal.pcbi.1005417.

[31] Yanping Xiao and Gordon J. Freeman. The microsatellite instable subset of colorectal cancer is a particularly good candidate for checkpoint blockade immunotherapy. *Cancer Discovery*, 5(1):16–18, 2015. ISSN 21598290. doi: 10.1158/2159-8290.CD-14-1397.

[32] Gina Columbus. Expert Discusses Microsatellite Instability, Immunotherapy in CRC. `http://www.onclive.com/web-exclusives/expert-discusses-microsatel` 2016. [Online; accessed 2016-12-06].

[33] Steven A Rosenberg. Interleukin 2 for patients with renal cancer. *Nature clinical practice. Oncology*, 4(9):497, 2007. ISSN 1743-4262. doi: 10.1038/ncponc0926.

[34] Martin Reck, Delvys Rodríguez-Abreu, Andrew G. Robinson, Rina Hui, Tibor Csoszi, Andrea Fülöp, Maya Gottfried, Nir Peled, Ali Tafreshi, Sinead Cuffe, Mary O'Brien, Suman Rao, Katsuyuki Hotta, Melanie A. Leiby, Gregory M. Lubiniecki, Yue Shentu, Reshma Rangwala, and Julie R. Brahmer. Pembrolizumab versus Chemotherapy for PD-L1–Positive Non–Small-Cell Lung Cancer. *New England Journal of Medicine*, 375(19):1823–1833, 2016. ISSN 0028-4793. doi: 10.1056/NEJMoa1606774.

[35] Chris Fellner. Ipilimumab (Yervoy) Prolongs Survival In Advanced Melanoma. *P&T*, 37(9):503–512, 2012. ISSN 1052-1372.

[36] A Amin and RL White. Interleukin-2 in Renal Cell Carcinoma: A Has-Been or a Still-Viable Option? *Journal of Kidney Cancer and VHL*, 1(7):74–83, 2014. doi: 10.15586/jkcvhl.2014.18.

[37] M E Smith and W L Ford. The recirculating lymphocyte pool of the rat: a systematic description of the migratory behaviour of recirculating lymphocytes. *Immunology*, 49(1):83–94, 1983. ISSN 0019-2805.

[38] Michael H. Kershaw, Jennifer A. Westwood, Linda L. Parker, Gang Wang, Zelig Eshhar, Sharon A. Mavroukakis, Donald E. White, John R. Wunderlich, Silvana Canevari, Linda Rogers-Freezer, Clara C. Chen, James C. Yang, Steven A. Rosenberg, and Patrick Hwu. A Phase I Study on Adoptive Immunotherapy Using Gene-Modified T Cells for Ovarian Cancer. *Clinical Cancer Research*, 12(20):6106–6115, 2006. ISSN 1078-0432. doi: 10.1158/1078-0432.CCR-06-1183.

[39] Ana Caterina Parente-Pereira, Jerome Burnet, David Ellison, Julie Foster, David Marc Davies, Sjoukje Van der Stegen, Sophie Burbridge, Laura Chiapero-Stanke, Scott Wilkie, Stephen Mather, and John Maher. Trafficking of CAR-Engineered Human T Cells Following Regional or Systemic Adoptive Transfer in SCID Beige Mice. *Journal of Clinical Immunology*, 31(4):710–718, 2011. doi: 10.1007/s10875-011-9532-8.

[40] Tapani Lahtinen, Paavo Karjalainen, and Esko M. Alhava. Measurement of bone blood flow with a 133Xe washout method. *European Journal of Nuclear Medicine*, 4:437, 1979.

[41] Christoph Scheiermann, Julie Gibbs, Louise Ince, and Andrew Loudon. Clocking in to immunity. *Nature Reviews Immunology*, 18:423–437, 2018. doi: 10.1038/s41577-018-0008-4.

[42] Linan Wang, Ning Ma, Sachiko Okamoto, Yasunori Amaishi, Eiichi Sato, Naohiro Seo, Junichi Mineno, Kazutoh Takesako, Takuma Kato, and Hiroshi Shiku. Efficient tumor regression by adoptively transferred CEA-specific CAR-T cells associated with symptoms of mild cytokine release syndrome. *OncoImmunology*, 5(9):1–13, 2016. ISSN 2162402X. doi: 10.1080/2162402X.2016.1211218.

[43] Markus Chmielewski, Olga Hahn, Gunter Rappl, Michael Nowak, Ingo H. Schmidt-Wolf, Andreas A. Hombach, and Hinrich Abken. T cells that target carcinoembryonic antigen eradicate orthotopic pancreatic carcinomas without inducing autoimmune colitis in mice. *Gastroenterology*, 143(4):1095–1107.e2, 2012. ISSN 00165085. doi: 10.1053/j.gastro.2012.06.037.

[44] Chengcheng Zhang, Zhe Wang, Zhi Yang, Meiling Wang, Shiqi Li, Yunyan Li, Rui Zhang, Zhouxing Xiong, Zhihao Wei, Junjie Shen, Yongli Luo, Qianzhen Zhang, Limei Liu, Hong Qin, Wei Liu, Feng Wu, Wei Chen, Feng Pan, Xianquan Zhang, Ping Bie, Houjie Liang, Gabriele Pecher, and Cheng Qian. Phase I Escalating-Dose Trial of CAR-T Therapy Targeting CEA+Metastatic Colorectal Cancers. *Molecular Therapy*, 25(5):1248–1258, 2017. ISSN 15250024. doi: 10.1016/j.ymthe.2017.03.010.

[45] Shan-Shan Jiang, Yan Tang, Yao-Jun Zhang, D-Sheng Weng, Zhong-Guo Zhou, Ke Pan, Qiu-Zhong Pan, Qi-Jing Wang, Qing Liu, Jia He, Jing-Jing Zhao, Jiang Li, Min-Shan Chen, Alfred E Chang, Qiao Li, and Jian-Chuan Xia. A phase I clinical trial utilizing autologous tumor-infiltrating lymphocytes in patients with primary hepatocellular carcinoma. *Oncotarget*, 6(38):41339–49, 2015. ISSN 1949-2553. doi: 10.18632/oncotarget.5463.

[46] M. H. Geukes Foppen, M. Donia, I. M. Svane, and J. B.A.G. Haanen. Tumor-infiltrating lymphocytes for the treatment of metastatic cancer. *Molecular Oncology*, 9(10):1918–1935, 2015. ISSN 18780261. doi: 10.1016/j.molonc.2015.10.018.

[47] Richard A Morgan, Mark E Dudley, John R Wunderlich, Marybeth S Hughes, James C Yang, Richard M Sherry, Richard E Royal, Suzanne L Topalian, Udai S Kammula, Nicholas P Restifo, Zhili Zheng, Azam Nahvi, Christiaan R De Vries, Linda J Rogers-freezer, Sharon A Mavroukakis, and Steven A Rosenberg. Cancer Regression in Patients. *In Vitro*, 126(2006):126–130, 2007. doi: 10.1126/science.1129003.

[48] Eric Tran, Paul F. Robbins, Yong-Chen Lu, Todd D. Prickett, Jared J. Gartner, Li Jia, Anna Pasetto, Zhili Zheng, Satyajit Ray, Eric M. Groh, Isaac R. Kriley, and Steven A. Rosenberg. T-Cell Transfer Therapy Targeting Mutant KRAS in Cancer. *New England Journal of Medicine*, 375(23):2255–2262, 2016. ISSN 0028-4793. doi: 10.1056/NEJMoa1609279.

[49] F. Kallinowski, K. H. Schlenger, S. Runkel, M. Kloes, M. Stohrer, P. Okunieff, and P. Vaupel. Blood Flow, Metabolism, Cellular Microenvironment, and Growth Rate of Human Tumor Xenografts. *Cancer Res.*, 49(14):3759–3764, 1989. ISSN 0008-5472.

[50] Cassandra Willyard. The mice with human tumours: Growing pains for a popular cancer model. *Nature*, 560:156–157, 2018. doi: 10.1038/d41586-018-05890-8.

[51] Rebar N. Mohammed, H. Angharad Watson, Miriam Vigar, Julia Ohme, Amanda Thomson, Ian R. Humphreys, and Ann Ager. L-selectin Is Essential for Delivery of Activated CD8+ T Cells to Virus-Infected Organs for Protective Immunity. *Cell Reports*, 14(4):760–771, 2016. ISSN 22111247. doi: 10.1016/j.celrep.2015.12.090.

[52] David Masopust and Jason M. Schenkel. The integration of T cell migration, differentiation and function. *Nat. Rev. Immunol.*, 13(5):309–320, May 2013. ISSN 1474-1733. doi: 10.1038/nri3442.

[53] Javier Mestas and Christopher C. W. Hughes. Of Mice and Not Men: Differences between Mouse and Human Immunology. *J. Immunol.*, 172(5):2731–2738, Mar 2004. ISSN 0022-1767. doi: 10.4049/jimmunol.172.5.2731.

[54] Ruud P. M. Dings, Melissa Loren, Hanke Heun, Elizabeth McNiel, Arjan W. Griffioen, Kevin H. Mayo, and Robert J. Griffin. Scheduling of Radiation with Angiogenesis Inhibitors Anginex and Avastin Improves Therapeutic Outcome via Vessel Normalization. *Clin. Cancer Res.*, 13(11):3395–3402, Jun 2007. ISSN 1078-0432. doi: 10.1158/1078-0432.CCR-06-2441.

[55] Limor Amit, Irit Ben-Aharon, Liat Vidal, Leonard Leibovici, and Salomon Stemmer. The Impact of Bevacizumab (Avastin) on Survival in Metastatic Solid Tumors - A Meta-Analysis and Systematic Review. *PLoS One*, 8(1):e51780, Jan 2013. ISSN 1932-6203. doi: 10.1371/journal.pone.0051780.

[56] Cor H.J. Lamers, Yarne Klaver, Jan W. Gratama, Stefan Sleijfer, and Reno Debets. Treatment of metastatic renal cell carcinoma (mRCC) with CAIX CAR-engineered T-cells–a completed study overview. *Biochemical Society Transactions*, 44(3):951–959, 2016. ISSN 0300-5127. doi: 10.1042/BST20160037.

List of Figures

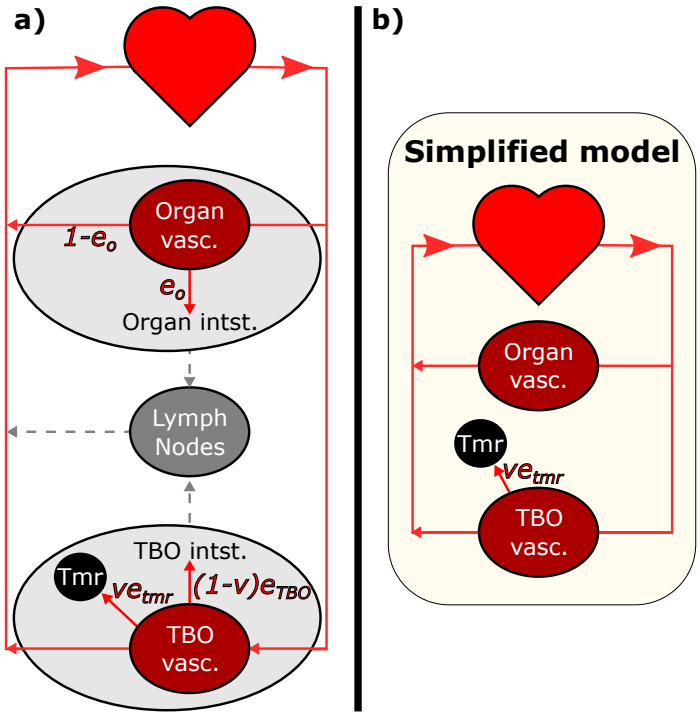

Figure 1. Model schematic: a) A visual summary of the presented model. Solid and dotted lines represent blood and lymph flow respectively. Cells flow from the heart to each organ o, from which a proportion e_o enters the interstitial space. Cells from the interstitium flow via the lymphatics back to the heart. One organ is designated as the tumour bearing organ (TBO), from which a proportion of cells ve_{tmr} extravasate irreversibly to the tumour ("Tmr") instead of the organ interstitium, where $v = \frac{V_{\text{tmr}}}{V_{\text{TBO}}}$ is the proportion of the TBO volume taken up by the tumour. **b)** When calculating the maximum rate of extravasation to a tumour by organ, a simplified version of the model that ignores the interstitial space may be used, as shown on the right. In both schematics, extra details such as the spleen or flow from the mesentery to the liver are not shown; see supplementary section 1.1.

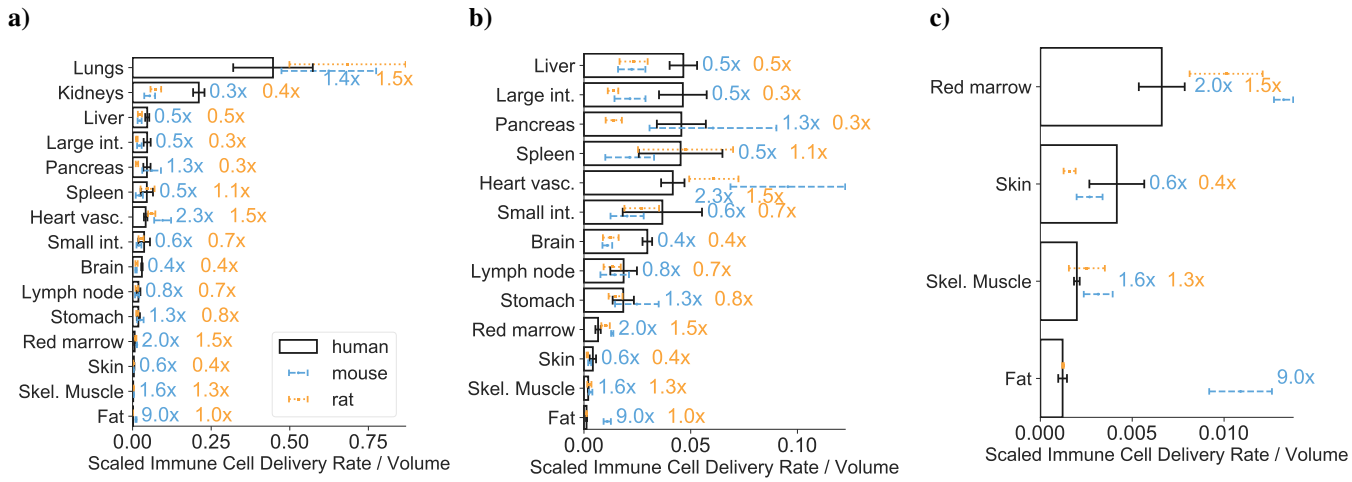

Figure 2. a) Relative predicted delivery rates for humans, rats and mice. Rates within each species were normalised to sum to 1.0 to give relative values for comparison. See Table 1 for a comparison of absolute rates. Predictions are presented as a mean and standard deviation over 100 repeats, with random fractional blood flows and volumes uniformly drawn from experimental data in the literature. Numerical values (text labels) give the mean predicted delivery rates in rats and mice relative to human values, with colours matching the legend. The relative distribution of rates across the major organs differs by species, and, consequently, inter-species scaling of delivery rates is organ-specific. **b,c)** Copies of plot **a** with successively fewer organs, to increase visibility of organs with lower delivery rates. Blue and orange colours have the same meaning as in plot **a**.

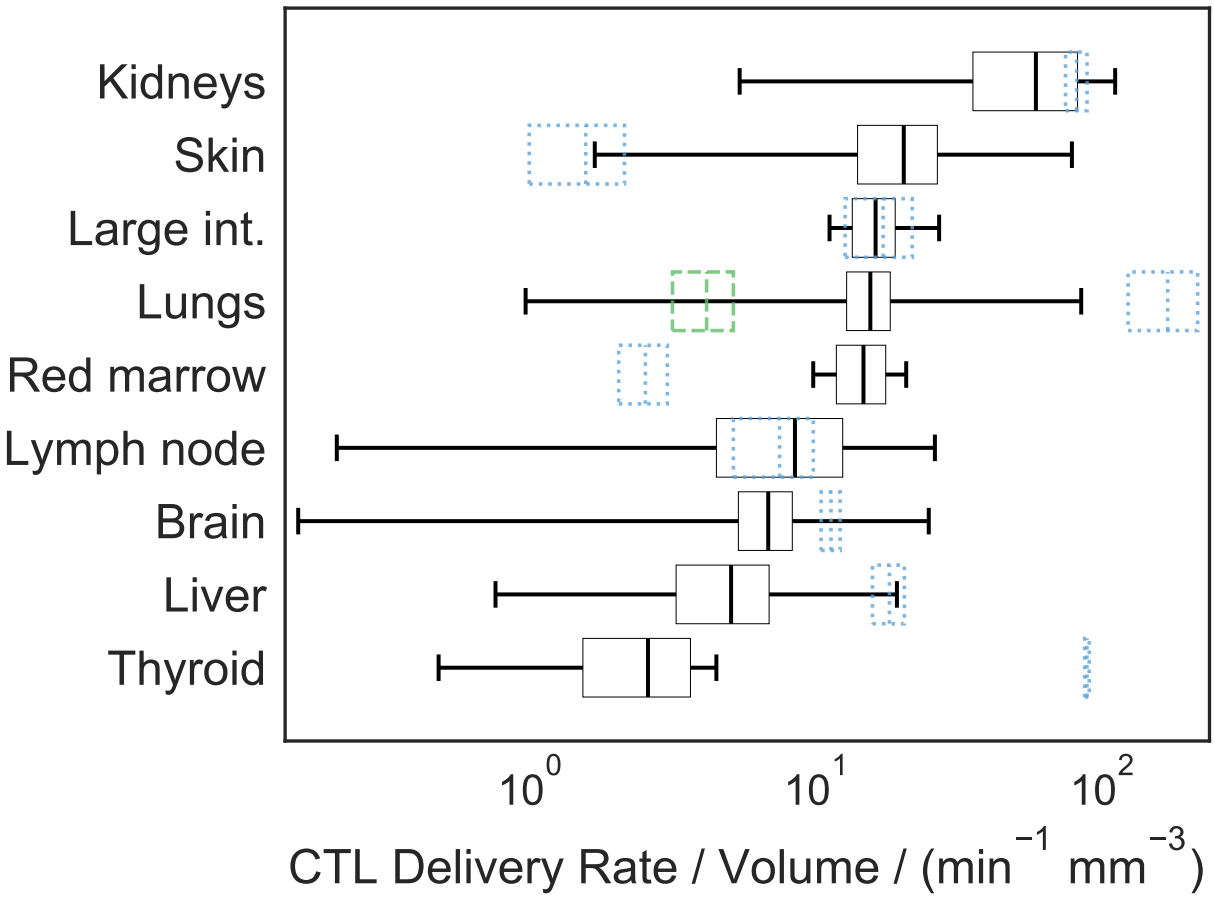

Figure 3. Absolute predicted delivery rates for human tumours, assuming 10^8 CART-cells are administered IV. Predictions are presented as a mean and standard deviation over 150 repeats, with random anatomical parameters and tumour perfusion drawn from experimental data in the literature. Black boxes represent the mean and standard deviation of predicted tumour delivery rates, and whiskers indicate predictions using the extremes of possible tumour perfusion according to the literature. Blue dotted boxes indicate the mean and standard deviation of predicted delivery to healthy tissue, *i.e.* the data used to generate Figure 2. The green dashed box indicates delivery rates per mm^3 to healthy lung tissue when the pulmonary circuit is assumed not to contribute. Note that now the kidneys and skin have the highest predicted tumour delivery rates, and that the horizontal axis is a log scale.

a)

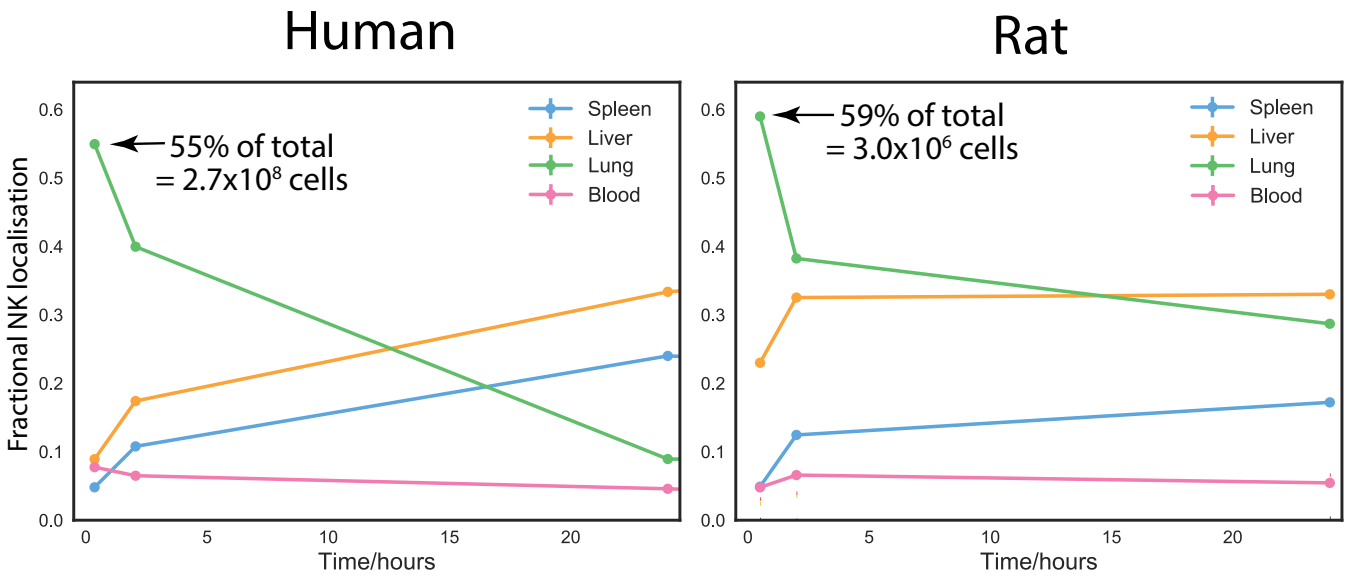

b)

	Lung		Liver		Spleen	
	Human	**Rat**	**Human**	**Rat**	**Human**	**Rat**
Organ fraction after 30 mins	55.0%	59.0%	8.9%	23.0%	4.8%	4.9%
Number of cells in organ	2.7×10^8	3.0×10^6	4.5×10^7	1.2×10^6	2.4×10^7	2.5×10^5
Number scaled by dose	2.7×10^8	3.0×10^8	0.45×10^8	1.2×10^8	0.24×10^8	0.25×10^8
Number of cells / organ volume	2.4×10^5	3.0×10^8	2.6×10^4	1.1×10^7	1.7×10^5	4.1×10^7
Ratio of rat to human	1226		429		245	
Ratio of predicted delivery rates	2437		546		485	
Delivery ratio/localisation ratio	1.99		1.27		1.98	

Figure 4. A comparison of reported localisation of radiolabelled natural killer (NK) cells in rats and humans to model predictions [27–29]. **a)** Reproductions of the reported data, after normalising data at each time point such that the total radioactivity (localisation) is 1.0 at all time points. Annotations indicate the initial count of cells in the lung in each species. **b)** Analysis of the data. The dosage and fractional localisation in each organ can be used to calculate the number of NK cells present in each organ at each time point. By accounting for the different dose given to each species and choosing an appropriate estimate for organ volumes in each species, the number of cells per volume in each species can be calculated. The rat/human ratio of the number of cells in each organ can be compared to the ratio of maximum delivery rates per volume predicted by the model, obtained from Table 1.

List of Tables

Organ	Human	Mouse	Rat
Lungs	177.0	3,096,980	431,266
Kidneys	106.7	262,449	31,715
Thymus	53.6	265,913	26,619
Small intestine	31.3	161,379	16,715
Pancreas	28.6	130,298	13,289
Spleen	27.9	130,468	13,545
Large intestine	22.8	111,698	11,540
Liver	22.5	112,735	12,302
Heart vasculature	22.1	477,504	31,001
Brain	14.4	49,485	6,005
Lymph node	13.0	29,731	3,064
Stomach	12.3	6,685	19,417
Red marrow	9.3	116,958	7,010
Skin	3.3	11,286	840.6
Skeletal muscle	1.1	15,525	1,590
Fat	0.8	13,790	1,419

Table 1. Predicted absolute maximum CART-cell delivery rates per volume (cells/min/mm^3) by organ and species, assuming homogeneous organ perfusion, that 10^8 CART-cells are introduced to each species and using previously compiled physiological parameter values [22]. The interspecies differences in absolute delivery rates per volume depend only on organ perfusion.

Organ	**Equivalent dose**	**(continued)**	
Lungs	1.7×10^{11}	Heart vasculature	2.2×10^{11}
Kidneys	2.5×10^{10}	Brain	3.4×10^{10}
Thymus	5.0×10^{10}	Lymph node	2.3×10^{10}
Small intestine	5.2×10^{10}	Stomach	5.4×10^{09}
Pancreas	4.6×10^{10}	Red marrow	1.3×10^{11}
Spleen	4.7×10^{10}	Skin	3.4×10^{10}
Large intestine	4.9×10^{10}	Skeletal muscle	1.4×10^{11}
Liver	5.0×10^{10}	Fat	1.7×10^{11}

Table 2. The dosage of CART-cells in humans predicted to be required to give the same absolute delivery rate per mm^3 as in a mouse given 10^7 cells. The numbers required are much larger than many clinical dosages [25, 26].